

Measurement of the $^{76}\text{Ge}(n, \gamma)$ cross section at the n_TOF facility at CERN

A. Gawlik-Ramięga^{1,*}, C. Lederer-Woods,² M. Krtička,³ S. Valenta,³ U. Battino,² J. Andrzejewski,¹ J. Perkowski,¹ O. Aberle,⁴ L. Audouin,⁵ M. Bacak,⁶ J. Balibrea,⁷ M. Barbagallo,⁸ S. Barros,⁹ V. Bécaries,⁷ F. Bečvář,³ C. Beinrucker,¹⁰ E. Berthoumieux,¹¹ J. Billowes,¹² D. Bosnar,¹³ M. Brugger,⁴ M. Caamaño,¹⁴ F. Calviño,¹⁵ M. Calviani,⁴ D. Cano-Ott,⁷ R. Cardella,⁴ A. Casanovas,¹⁵ D. M. Castelluccio,^{16,17} F. Cerutti,⁴ Y. H. Chen,⁵ E. Chiaveri,⁴ N. Colonna,⁸ G. Cortés,¹⁵ M. A. Cortés-Giraldo,¹⁸ L. Cosentino,¹⁹ L. A. Damone,^{8,20} M. Diakaki,¹¹ M. Dietz,² C. Domingo-Pardo,²¹ R. Dressler,²² E. Dupont,¹¹ I. Durán,¹⁴ B. Fernández-Domínguez,¹⁴ A. Ferrari,⁴ P. Ferreira,⁹ P. Finocchiaro,¹⁹ V. Furman,²³ K. Göbel,¹⁰ A. R. García,⁷ T. Glodariu,^{24,†} I. F. Gonçalves,⁹ E. González-Romero,⁷ A. Goverdovski,²⁵ E. Griesmayer,⁶ C. Guerrero,¹⁸ F. Gunsing,^{11,4} H. Harada,²⁶ T. Heftrich,¹⁰ S. Heinitz,²² J. Heyse,²⁷ D. G. Jenkins,²⁸ E. Jericha,⁶ F. Käppeler,²⁹ Y. Kadi,⁴ T. Katabuchi,³⁰ P. Kavrigin,⁶ V. Ketlerov,²⁵ V. Khryachkov,²⁵ A. Kimura,²⁶ N. Kivel,²² I. Knapová,³ M. Kokkoris,³¹ E. Leal-Cidoncha,¹⁴ H. Leeb,⁶ J. Leredegui-Marco,¹⁸ S. Lo Meo,^{16,17} S. J. Lonsdale,² R. Losito,⁴ D. Macina,⁴ T. Martínez,⁷ C. Massimi,^{17,32} P. Mastinu,³³ M. Mastromarco,⁸ F. Matteucci,^{34,35} E. A. Maugeri,²² E. Mendoza,⁷ A. Mengoni,¹⁶ P. M. Milazzo,³⁴ F. Mingrone,¹⁷ M. Mirea,^{24,†} S. Montesano,⁴ A. Musumarra,^{19,36} R. Nolte,³⁷ A. Oprea,²⁴ N. Patronis,³⁸ A. Pavlik,³⁹ J. I. Porras,^{4,40} J. Praena,⁴⁰ J. M. Quesada,¹⁸ K. Rajeev,⁴¹ T. Rauscher,^{42,43} R. Reifarh,¹⁰ A. Riego-Perez,¹⁵ P. C. Rout,⁴¹ C. Rubbia,⁴ J. A. Ryan,¹² M. Sabaté-Gilarte,^{4,18} A. Saxena,⁴¹ P. Schillebeeckx,²⁷ S. Schmidt,¹⁰ D. Schumann,²² P. Sedyshev,²³ A. G. Smith,¹² A. Stamatopoulos,³¹ G. Tagliente,⁸ J. L. Tain,²¹ A. Tarifeño-Saldivia,^{15,21} L. Tassan-Got,⁵ A. Tattersall,² A. Tsinganis,³¹ G. Vannini,^{17,32} V. Variale,⁸ P. Vaz,⁹ A. Ventura,¹⁷ V. Vlachoudis,⁴ R. Vlastou,³¹ A. Wallner,⁴⁴ S. Warren,¹² M. Weigand,¹⁰ C. Weiss,^{4,6} C. Wolf,¹⁰ P. J. Woods,² T. Wright,¹² and P. Žugec^{13,4}

(n_TOF Collaboration)

¹University of Lodz, Poland²School of Physics and Astronomy, University of Edinburgh, United Kingdom³Charles University, Prague, Czech Republic⁴European Organization for Nuclear Research (CERN), Switzerland⁵Institut de Physique Nucléaire, CNRS-IN2P3, Univ. Paris-Sud, Université Paris-Saclay, F-91406 Orsay Cedex, France⁶Technische Universität Wien, Austria⁷Centro de Investigaciones Energéticas Medioambientales y Tecnológicas (CIEMAT), Spain⁸Istituto Nazionale di Fisica Nucleare, Sezione di Bari, Italy⁹Instituto Superior Técnico, Lisbon, Portugal¹⁰Goethe University Frankfurt, Germany¹¹CEA Irfu, Université Paris-Saclay, F-91191 Gif-sur-Yvette, France¹²University of Manchester, United Kingdom¹³Department of Physics, Faculty of Science, University of Zagreb, Zagreb, Croatia¹⁴University of Santiago de Compostela, Spain¹⁵Universitat Politècnica de Catalunya, Spain¹⁶Agenzia nazionale per le nuove tecnologie (ENEA), Bologna, Italy¹⁷Istituto Nazionale di Fisica Nucleare, Sezione di Bologna, Italy¹⁸Universidad de Sevilla, Spain¹⁹INFN Laboratori Nazionali del Sud, Catania, Italy²⁰Dipartimento di Fisica, Università degli Studi di Bari, Italy²¹Instituto de Física Corpuscular, CSIC - Universidad de Valencia, Spain²²Paul Scherrer Institut (PSI), Villigen, Switzerland²³Joint Institute for Nuclear Research (JINR), Dubna, Russia²⁴Horia Hulubei National Institute of Physics and Nuclear Engineering, Romania²⁵Institute of Physics and Power Engineering (IPPE), Obninsk, Russia²⁶Japan Atomic Energy Agency (JAEA), Tokai-mura, Japan²⁷European Commission, Joint Research Centre (JRC), Retieseweg 111, B-2440 Geel, Belgium²⁸University of York, United Kingdom²⁹Karlsruhe Institute of Technology, Campus North, IKP, 76021 Karlsruhe, Germany³⁰Tokyo Institute of Technology, Japan

* aleksandra.gawlik@uni.lodz.pl

† Deceased.

³¹*National Technical University of Athens, Greece*³²*Dipartimento di Fisica e Astronomia, Università di Bologna, Italy*³³*Istituto Nazionale di Fisica Nucleare, Sezione di Legnaro, Italy*³⁴*Istituto Nazionale di Fisica Nucleare, Sezione di Trieste, Italy*³⁵*Dipartimento di Astronomia, Università di Trieste, Italy*³⁶*Dipartimento di Fisica e Astronomia, Università di Catania, Italy*³⁷*Physikalisch-Technische Bundesanstalt (PTB), Bundesallee 100, 38116 Braunschweig, Germany*³⁸*University of Ioannina, Greece*³⁹*University of Vienna, Faculty of Physics, Vienna, Austria*⁴⁰*University of Granada, Spain*⁴¹*Bhabha Atomic Research Centre (BARC), India*⁴²*Centre for Astrophysics Research, University of Hertfordshire, United Kingdom*⁴³*Department of Physics, University of Basel, Switzerland*⁴⁴*Australian National University, Canberra, Australia*

(Received 24 June 2021; accepted 27 September 2021; published 12 October 2021)

The ${}^{76}\text{Ge}(n, \gamma)$ reaction has been measured at the n_TOF facility at CERN via the time-of-flight technique. Neutron capture cross sections on ${}^{76}\text{Ge}$ are of interest to a variety of low-background experiments, such as neutrinoless double β decay searches, and to nuclear astrophysics. We have determined resonance capture kernels up to 52 keV neutron energy and used the new data to calculate Maxwellian-averaged neutron capture cross sections for $k_{\text{B}}T$ values of 5 to 100 keV.

DOI: [10.1103/PhysRevC.104.044610](https://doi.org/10.1103/PhysRevC.104.044610)

I. MOTIVATION

High-precision neutron capture data on ${}^{76}\text{Ge}$ are of interest for fundamental research in nuclear astrophysics and for low-background experiments in the search of neutrinoless double β decay.

In nuclear astrophysics, neutron capture cross sections are a key input for studying the origin of the heavy elements in the slow neutron capture process (*s* process) [1]. About 80% of solar elemental germanium is thought to be produced in the *s* process in massive stars during He core burning (at temperature $k_{\text{B}}T \approx 30$ keV) and neutron densities of about 10^6 n/cm³ [2], and then during the later C shell burning phase (at temperature $k_{\text{B}}T \approx 90$ keV) with significantly higher neutron densities around 10^{12} n/cm³ [2]. Figure 1 shows the reaction path of the *s* process in massive stars in the mass region around germanium. ${}^{76}\text{Ge}$ is preceded by the unstable ${}^{75}\text{Ge}$, with a half-life of only 83 minutes. During He core burning, neutron densities are too low to cause significant capture on ${}^{75}\text{Ge}$, hence the pre-existing ${}^{76}\text{Ge}$ is thought to be mainly destroyed by (*n, γ*) reactions. During the later C shell burning stage, higher neutron densities allow production of ${}^{76}\text{Ge}$, which may compensate for its destruction in the previous phase [3]. Hence, in the *s* process in massive stars, ${}^{76}\text{Ge}$ is either destroyed or marginally produced. Therefore, ${}^{76}\text{Ge}$ is commonly considered as so-called *r*-only nucleus, meaning that it is dominantly produced in the rapid neutron capture process happening in stellar explosions, such as neutron-star mergers [4]. Nevertheless, accurate neutron capture data on ${}^{76}\text{Ge}$ are needed to determine the destruction of ${}^{76}\text{Ge}$ during the *s* process, and its possible contribution to galactic chemical evolution.

Furthermore, ${}^{76}\text{Ge}$ is commonly used as a probe in the hunt of neutrinoless double β decay, for instance at GERDA [5], MJD [6], and the future LEGEND [7] experiments. Neutron

interactions represent an important source of background in these searches [8], so an accurate neutron reaction data on ${}^{76}\text{Ge}$ is thus of importance to model backgrounds.

Experimental neutron capture cross-section data on ${}^{76}\text{Ge}$ are scarce. There are several measurements at thermal-neutron energies (0.025 eV) [9–12]. Data at higher neutron energies include resonance data by Maletski *et al.* [13], who have measured partial radiative widths only for two resonances below 5 keV. Cross sections recommended by nuclear data libraries such as ENDF/B-VIII [14] and JEFF-3.3 [15] are based on experimental data of Ref. [13], in combination with transmission data on natural germanium by Harvey and Hockaday [16]. However, the data include only a few of the strongest resonances, due to the low natural abundance of ${}^{76}\text{Ge}$ ($\approx 8\%$). At higher neutron energies, Bhike *et al.* [17] have recently published capture cross sections between 0.4 and 14.8 MeV, which were found to be in agreement with evaluations [14,18].

There exists also several measurements of Maxwellian-averaged cross sections (MACSs). The most recent, by Marganec *et al.* [19], have determined MACS at $k_{\text{B}}T = 25$ keV using the activation technique and extrapolated MACS values from $k_{\text{B}}T = 5$ –100 keV using the Bao *et al.* compilation [20]. Their results were found to be smaller than previous activation data at 25 keV obtained by Anand *et al.* [21], and Chaubey and Seghal [22].

This work presents neutron capture resonance data obtained at the n_TOF facility, providing for the first time information on individual resonance parameters relevant for radiative neutron capture on ${}^{76}\text{Ge}$ up to 52 keV. These resonance data were used to constrain average resonance parameters and Maxwellian averaged cross sections.

II. EXPERIMENT AT n_TOF

The n_TOF neutron time-of-flight facility consists of a neutron spallation source, and two experimental areas;

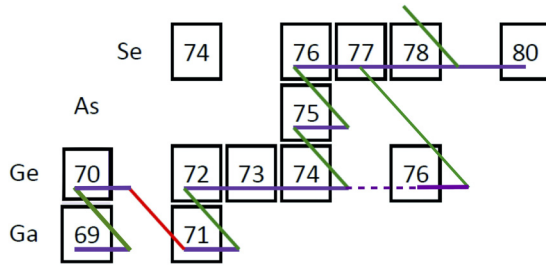


FIG. 1. Nucleosynthesis path of the s process going along the stability valley. Solid boxes represent stable isotopes. Neutron captures are marked by purple lines and β decays by green (β^-) and red (β^+) lines. There is only a marginal reaction flow to ^{76}Ge via $^{75}\text{Ge}(n, \gamma)$.

Experimental Area 1 (EAR-1) is located at a distance of 185 m from the target, while Experimental Area 2 (EAR-2) for measurements requiring ultrahigh neutron fluxes is located at a distance of 20 m [23]. Neutrons are produced in spallation reactions, by bombarding a cylindrical 1.3 ton lead target (40 cm length, 60 cm diameter) with a pulsed proton beam (7 ns rms), provided by the CERN Proton Synchrotron. The spallation target is surrounded by borated and normal water layers to moderate the initially energetic neutrons, reduce γ -induced backgrounds, and cool the spallation target [23]. The moderated neutron spectrum is characterized by an isolethargic energy dependence and ranges from thermal energies (25 meV) to several GeV. The measurement was performed at EAR-1, taking advantage of the excellent relative neutron energy resolution, which ranges from 3×10^{-4} at 1 eV to 3×10^{-3} at 100 keV [23].

Capture events were detected by measuring the prompt capture γ rays with four deuterated benzene (C_6D_6) liquid scintillators. These detectors have been specifically optimized for an extremely low sensitivity to scattered neutrons [24,25]. The detectors were placed symmetrically around the beam pipe at 125 degrees with respect to the neutron beam to minimize effects of anisotropic γ -ray emission for $\ell > 0$ capture. The ^{76}Ge sample, supplied by ISOFLEX (USA), consisted of GeO_2 in powder form enriched to 88.46% in ^{76}Ge . The sample was pressed into a self-supporting cylindrical pellet at the Paul Scherrer Institute (Switzerland). In addition, we also measured a metallic natural Ge sample to identify neutron resonances due to impurities from other isotopes. Data were also recorded with a ^{197}Au sample for normalizing the cross section (see Sec. III), and with an empty sample holder to determine the sample-independent background. All samples were of cylindrical shape with 2 cm diameter and were glued on to a 6- μm -thick Mylar foil, attached to a thin aluminium ring of 5 cm diameter. Table I gives properties of the samples used in our experiment.

TABLE I. Properties of the samples used in the measurement, all cylindrical with 2 cm diameter.

| Sample | Chemical form | Mass (g) | Thickness (mm) | Sample composition (%) |
|--------------------------|----------------|----------|----------------|---|
| ^{76}Ge | GeO_2 | 2.275 | 2.43 | $^{70}\text{Ge}(0.06)$; $^{72}\text{Ge}(0.09)$; $^{73}\text{Ge}(0.06)$; $^{74}\text{Ge}(11.33)$; $^{76}\text{Ge}(88.46)$ |
| $^{\text{nat}}\text{Ge}$ | Metal | 1.903 | 1.22 | $^{70}\text{Ge}(20.52)$; $^{72}\text{Ge}(27.45)$; $^{73}\text{Ge}(7.76)$; $^{74}\text{Ge}(36.52)$; $^{76}\text{Ge}(7.75)$ |
| ^{197}Au | Metal | 0.664 | 0.10 | $^{197}\text{Au}(100)$ |
| Empty holder | | | | |

Detector signals were recorded using 14-bit flash ADCs at a sampling rate of 1 GHz. Signal arrival times and amplitudes were determined with an off-line pulse shape algorithm, developed specifically for the detectors used [26].

III. DATA ANALYSIS AND RESULTS

A. Time to neutron energy conversion

The neutron time-of-flight spectra were converted to neutron energy using the relativistic relation

$$E_n = m_n c^2 (\gamma - 1), \quad (1)$$

with the Lorentz factor

$$\gamma = \frac{1}{\sqrt{1 - (L/t_{\text{tof}})^2/c^2}}, \quad (2)$$

where m_n is the mass of the neutron, L is the flight path length, and t_{tof} is the neutron time of flight. The time of neutron creation is inferred from measuring the so-called γ flash, a high-amplitude signal registered by the C_6D_6 detectors from prompt γ rays produced when the proton beam hits the spallation target. The flight path length was determined as 183.95 ± 0.04 m, using well-known neutron resonance energies in the $^{197}\text{Au}(n, \gamma)$ cross section [14].

B. Experimental capture yield

The experimental capture yield $Y(E_n)$ was obtained as follows:

$$Y(E_n) = f_N(E_n) \frac{C(E_n) - B(E_n)}{\epsilon_c \Phi(E_n)}, \quad (3)$$

where C is the count spectrum of ^{76}Ge sample, B is the background, ϵ_c is the detection efficiency, and Φ is the neutron fluence. The factor f_N is a normalization factor taking into account the fact that capture sample does not cover the entire size of the neutron beam. The determination of all the components will be described in the following sections. For all samples, dead time corrections were $\lesssim 1\%$.

1. Detection efficiency

The efficiency to detect a capture event depends on the specific deexcitation path of the compound system and therefore can vary for each neutron capture. To compensate for this feature, we used the well-established pulse-height weighting technique (PHWT) [27], which can be applied to detection systems where the detection efficiency ϵ_γ is low, and at most one γ ray per cascade is detected. If the γ -detection efficiency ϵ_γ is proportional to the γ -ray energy E_γ , it can be shown that the efficiency ϵ_c to detect a capture event is proportional

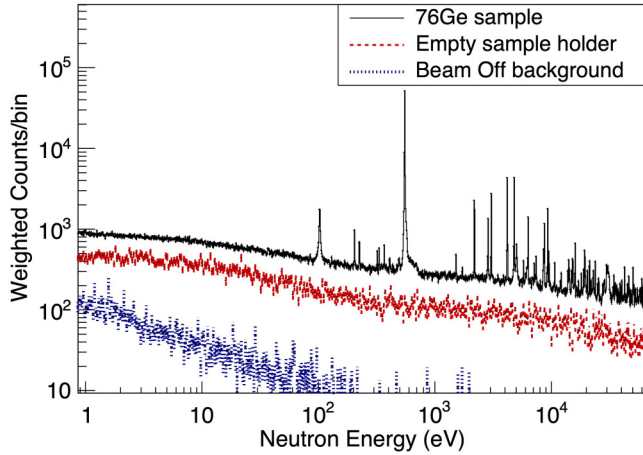


FIG. 2. Plot of the weighted ^{76}Ge spectrum compared with empty sample holder and ambient background.

to the excitation energy of the compound nucleus E_c . However, for most detection systems this is not the case, hence proportionality between ϵ_γ and E_γ is achieved by applying a pulse-height-dependent weight to each recorded signal. These weights were determined in detailed GEANT4 simulations [28] of the response of the detection setup to monoenergetic γ -ray energies over the energy range of interest, i.e., for all $E_\gamma \leq E_c$. Corrections for missed transitions due to γ rays below the 200 keV analysis threshold and transitions by electron conversion were calculated by using simulated cascades generated with the DICEBOX code [29]. The systematic uncertainty of the neutron capture yield due to the PHWT is 2% [30].

2. Background subtraction

Several sources of background affect our measured data. The environmental background caused by ambient radioactivity and cosmic rays is measured in runs without the neutron beam. Beam-induced background by neutron reactions on the sample holder and other structural material is measured with an empty sample holder. The ambient background has to be subtracted from each measured spectrum. The background B is calculated by subtracting the ambient component from the empty holder spectrum, all spectra have been weighted by a proper factors. Figure 2 shows the weighted ^{76}Ge count spectrum compared with these two background components. As mentioned above, the C_6D_6 detection setup has been optimized to have a low sensitivity to scattered neutrons [24,25].

3. Neutron fluence and normalisation

The neutron flux was accurately measured in a separate campaign [31] using nuclear reactions whose cross sections are considered a reference or standard in certain energy ranges. The energy-dependent neutron flux was determined with systematic uncertainty of 2% for neutron energies <10 keV, and of 4%–5% between 10 and 100 keV [31].

To determine the neutron fluence on the sample, a normalization factor f_N needs to be applied since the diameter of the neutron beam (3.5–4.0 cm) is larger than the diameter of the capture sample (2 cm). The normalization factor

TABLE II. Resonance energies E_R and kernels k up to 52 keV determined with SAMMY. The uncertainties listed originate only from the fitting procedure.

| E_R (eV) | k (meV) |
|---------------------|----------------|
| 551.199 ± 0.005 | 83.8 ± 0.3 |
| 2181.48 ± 0.03 | 24.0 ± 0.4 |
| 4168.92 ± 0.04 | 109 ± 2 |
| 4787.13 ± 0.07 | 206 ± 4 |
| 6284.32 ± 0.12 | 78 ± 3 |
| 8669.0 ± 0.3 | 131 ± 6 |
| 9262.54 ± 0.16 | 212 ± 7 |
| 9479.4 ± 0.3 | 61 ± 3 |
| 14058.4 ± 0.9 | 108 ± 8 |
| 15138 ± 4 | 175 ± 12 |
| 15867.3 ± 0.6 | 214 ± 11 |
| 19152.1 ± 1.4 | 171 ± 12 |
| 19234.5 ± 0.9 | 158 ± 10 |
| 20168.7 ± 1.5 | 85 ± 8 |
| 21055 ± 3 | 232 ± 19 |
| 23634.5 ± 1.6 | 153 ± 15 |
| 24658 ± 3 | 73 ± 13 |
| 28281 ± 3 | 74 ± 12 |
| 29489 ± 4 | 225 ± 29 |
| 30345 ± 3 | 154 ± 17 |
| 30680 ± 5 | 66 ± 15 |
| 30936 ± 4 | 67 ± 13 |
| 33505 ± 4 | 111 ± 19 |
| 33947 ± 7 | 100 ± 30 |
| 34000 ± 4 | 200 ± 30 |
| 34628 ± 4 | 102 ± 19 |
| 34851 ± 7 | 120 ± 30 |
| 35836 ± 3 | 260 ± 30 |
| 38396 ± 5 | 130 ± 20 |
| 38670 ± 5 | 110 ± 30 |
| 39602 ± 5 | 170 ± 40 |
| 41947 ± 5 | 400 ± 50 |
| 44441 ± 4 | 84 ± 17 |
| 45558 ± 4 | 260 ± 40 |
| 45734 ± 9 | 70 ± 30 |
| 45793 ± 5 | 120 ± 30 |
| 47270 ± 6 | 100 ± 20 |
| 49313 ± 8 | 200 ± 30 |
| 49434 ± 8 | 300 ± 60 |
| 50263 ± 6 | 190 ± 40 |
| 51655 ± 10 | 210 ± 50 |

f_N was determined using the well-established saturated resonance technique [32] using the ^{197}Au resonance at 4.9 eV neutron energy, with a systematic uncertainty of about 1%. Small corrections to this normalization have to be applied at other neutron energies, as the size of the neutron beam slightly depends on neutron energy. These corrections were determined in simulations and verified experimentally [23] and never exceeded 1.9% in the energy range of interest.

C. Resonance analysis

Neutron resonances from $^{76}\text{Ge}(n, \gamma)$ reactions SAMMY were fit with the multilevel, multichannel R -matrix code SAMMY [33].

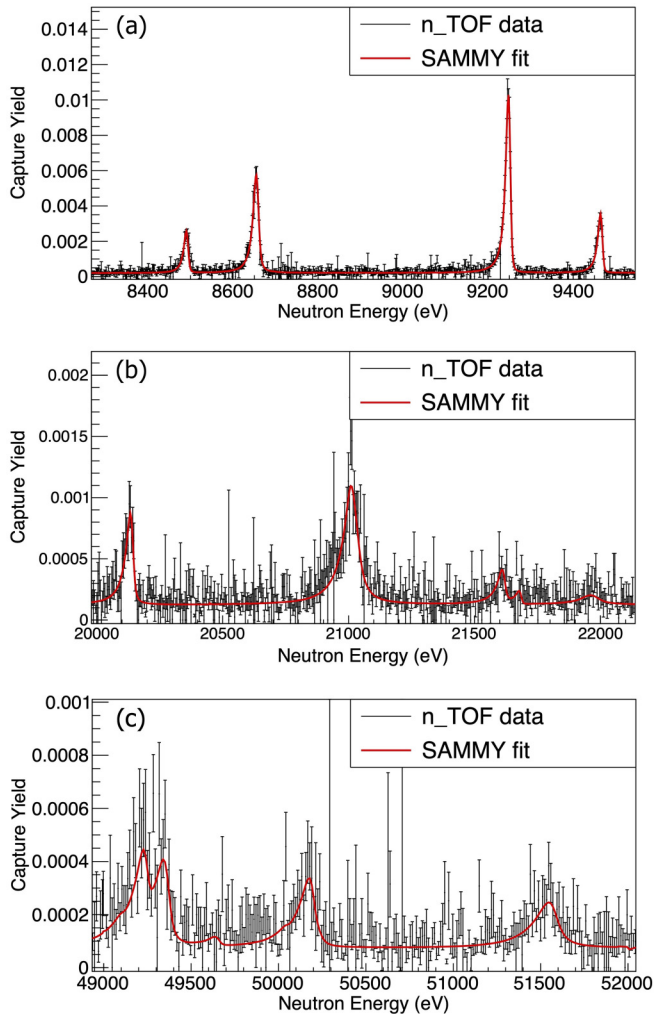


FIG. 3. (a)–(c) Examples for some SAMMY fits of the experimental capture yield.

SAMMY takes into account all experimental effects, such as self-shielding, multiple scattering, and the broadening of resonance shape due to thermal motion (Doppler broadening) and the resolution of the experimental setup. In addition, backgrounds introduced by sample impurities (i.e., other germanium isotopes) are included in calculations of resonance parameters. We also included a constant background in the fitting procedure to account for any residual background, by analogy with the previous Ge isotopes [34–36].

Table II lists our results for resonance energies and resonance capture kernels, defined as

$$k = g \frac{\Gamma_n \Gamma_\gamma}{\Gamma_n + \Gamma_\gamma}, \quad (4)$$

where Γ_n and Γ_γ are the neutron and radiative width, respectively. The statistical factor g is given by

$$g = \frac{(2J + 1)}{(2s + 1)(2I + 1)}, \quad (5)$$

where J is the resonance spin, $s = 1/2$ is the neutron spin, and $I(^{76}\text{Ge}) = 0$ is the ground-state spin of the target nucleus.

Resonance capture kernels were determined up to neutron energies of 52 keV. At higher energies, the analysis of indi-

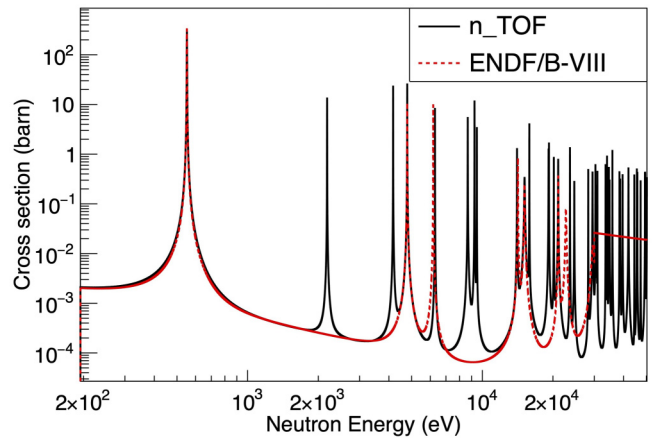


FIG. 4. ^{76}Ge neutron capture cross section reconstructed from SAMMY resonance fits in this work compared with ENDF/B-VIII [14].

vidual resonances is no longer possible due to the worsening of the experimental resolution combined with lower counting statistics. Examples for resonance fits of the capture yield using SAMMY are shown in Fig. 3. Resonances visible in Fig. 3 and not included in Table II come from other germanium isotopes, mainly from ^{74}Ge due to the high isotopic enrichment in the measured sample.

While the dependence of the kernel on the choice of resonance spin is negligible in most cases (i.e., kernel values for different J used in the SAMMY fit are consistent within uncertainties), the correct assignment of the resonance spin allows us to constrain average resonance parameters. For the ^{76}Ge reaction in the energy range investigated, it is expected that we observe s - and p -wave resonances, hence resonance spins J have values of either $1/2$ or $3/2$. Based on simulations with the DICEBOX code [29], we expect a similar $\bar{\Gamma}_\gamma$ for resonances with all allowed J^π . Since $\Gamma_n \gg \Gamma_\gamma$ for all but the three low-energy resonances, which results in a kernel $k \approx g\Gamma_\gamma$, we considered g , so that the resulting Γ_γ is distributed around the same value for different resonance spins. In our case, this means that all kernels $k > 180$ meV were fit as $J = 3/2$ resonances, while all others as $J = 1/2$ resonances.

Systematic uncertainties in the capture kernels are due to the PHWT (2%), the normalization (1%), the neutron flux (2% for $E_n < 10$ keV, 4.5% for $E_n > 10$ keV), and the sample enrichment (1%). This amounts to total systematic uncertainties of 3.2% below, and 5.1% above 10 keV neutron energy. In total, we determined 41 resonance kernels, the majority of them determined for the first time. The neutron capture cross section obtained from the resonance fits is shown in Fig. 4. The bound resonance parameters were taken from ENDF/B-VIII [14]. Using the results above, we are able to constrain the average resonance parameters, namely, the average radiative width $\bar{\Gamma}_\gamma$, the average resonance spacing D_0 , and neutron strength function S_0 . We assumed that there are no unresolved doublets or even more complex structures. We described the distribution of individual Γ_γ values in terms of the average radiative width $\bar{\Gamma}_\gamma$ and the width of the distribution σ_{Γ_γ} . Using the same method as in Ref. [35], namely, the maximum

TABLE III. Maxwellian-averaged cross sections obtained from resonance data below 52 keV neutron energy, combined with the data from libraries, and compared with previous measurement.

| $k_B T$ (keV) | MACS (mb) | | | | Ref. [19] |
|---------------|-------------------------|-------------|------------|------------------|------------|
| | This work | | | | |
| | n_TOF ($E_n < 52$ keV) | n_TOF+TALYS | n_TOF+ENDF | n_TOF+NON-SMOKER | |
| 5 | 65.0 ± 3.3 | 65.0 | 65.0 | 65.0 | 58.0 ± 5.8 |
| 10 | 37.9 ± 1.9 | 38.7 | 38.6 | 38.3 | 39.8 ± 3.4 |
| 20 | 20.5 ± 1.1 | 24.5 | 25.2 | 23.8 | 26.7 ± 2.3 |
| 25 | 16.1 ± 0.8 | 21.3 | 22.5 | 20.9 | 23.5 ± 2.0 |
| 30 | 13.0 ± 0.7 | 19.2 | 20.8 | 18.9 | 21.5 ± 1.8 |
| 40 | 8.9 ± 0.5 | 16.3 | 18.3 | 16.4 | 18.2 ± 1.5 |
| 50 | 6.5 ± 0.3 | 14.5 | 16.6 | 14.9 | 16.3 ± 1.4 |
| 60 | 4.9 ± 0.3 | 13.3 | 15.4 | 13.9 | 15.0 ± 1.3 |
| 70 | 3.8 ± 0.2 | 12.4 | 14.4 | 13.1 | |
| 80 | 3.09 ± 0.17 | 11.7 | 13.5 | 12.4 | 13.0 ± 1.1 |
| 90 | 2.53 ± 0.14 | 11.1 | 12.8 | 11.9 | |
| 100 | 2.12 ± 0.12 | 10.7 | 12.2 | 11.4 | 12.3 ± 1.1 |

likelihood fit assuming a Gaussian distribution of Γ_γ values, we obtained $\bar{\Gamma}_\gamma = 115(6)$ meV and $\sigma_{\Gamma_\gamma} = 30(4)$. Our value of the average radiative width is in excellent agreement with 115(25) meV of Mughabghab [37].

To determine D_0 we adopted a method similar to that used in the analysis of recently measured $^{73,70,72}\text{Ge}$ isotopes [34–36]. We compared the observed number of resonances having a kernel higher than 60 meV with predictions of simulations based on the statistical model, i.e., assuming a Porter-Thomas distribution of reduced neutron widths and Wigner spacing of neighboring resonances. The Γ_γ in simulations were assumed to have a common expectation value for all J^π and to originate from a χ_ν^2 distribution with $\nu = 30$ degrees of freedom; such a ν gives $\sigma_{\Gamma_\gamma}/\bar{\Gamma}_\gamma \approx 1/4$, in agreement with the values determined from the experiment. For the average level spacing we further assumed the spin dependence from Ref. [38] and parity independence. Our data give $D_0 = 4.6(6)$ keV, which is compatible with literature values of 3.6(9) keV [37] and 4.5(10) keV [39]. Although spin-parity assignment is uncertain, our data indicate a S_0 that is likely significantly smaller in this nucleus than in other germanium isotopes. Specifically, assuming that the highest deduced Γ_n/\sqrt{E} values correspond to s -wave resonances, we get $S_0 \approx 0.5 \times 10^{-4}$. The listed value can be considered as an upper limit because it was obtained from the strongest 15 resonances. In reality, some of these resonances are likely p waves, and from D_0 determined above there are only 12 expected s -wave resonances below 52 keV. The uncertainty in S_0 from Porter-Thomas distribution of reduced neutron widths is expected to be about 40%.

IV. STELLAR CROSS SECTIONS

Maxwellian-averaged cross sections (MACSs) were calculated for $k_B T$ values between 5 and 100 keV using the formula

$$\text{MACS} = \frac{2}{\sqrt{\pi}} \frac{1}{(k_B T)^2} \int_0^\infty E \sigma(E) \exp\left(-\frac{E}{k_B T}\right) dE. \quad (6)$$

Table III lists Maxwellian-averaged cross sections obtained from our data ($E_n < 52$ keV) and total (statistical and systematic) uncertainties. The systematic uncertainty in the MACS is 5.1% (see Sec. III C), while the statistical uncertainty is at most 2%. We also included a negative resonance [14] in our calculation, however, the contribution to the MACS is negligible (0.01% at $k_B T = 5$ keV and smaller for the higher $k_B T$). To determine the MACS including all relevant neutron energies, we have combined our data with theoretical predictions of the cross section from 52 keV to 1 MeV. We present MACS values using TALYS 1.9 with default parametrization [18], ENDF-B/VIII [14] and NON-SMOKER 5.3 [40]. MACS values at 5 and 10 keV are almost entirely determined by the experimental data and TALYS predictions of MACS for $k_B T \leq 10$ keV agree the best (within 7%). Therefore, we have used this combination for our astrophysical calculations. The table also lists the MACS values of Marganiec *et al.* [19]. They come from an activation measurement performed relative to the $^{197}\text{Au}(n, \gamma)$ cross section which has since been updated. Using the most recent $^{197}\text{Au}(n, \gamma)$ cross section [41–43], the MACS of Ref. [19] are to be multiplied by 1.078.

Stellar models suggest that, for low-metallicity stars, a small net production of ^{76}Ge in the s process is possible. At s -process burning temperatures around 30 and 90 keV, respectively, our new MACS values are about 12% smaller than the MACSs used in stellar models so far (these models adopt recommended values from the Karlsruhe Astrophysical Database of Nucleosynthesis in Stars (KADoNiS-0.3) [44], which corresponds to values from Ref. [19]). We have tested the impact of our results (adopting the n_TOF+TALYS MACSs) on s -process nucleosynthesis in a star with $25M_\odot$ initial mass and 0.6% metallicity, using the MESA stellar evolution code [45] in combination with the postprocessing code MPPNP [46]. This model yields a small net production of ^{76}Ge during s -process nucleosynthesis. The MACSs in this work lead to a marginal increase of the ^{76}Ge abundance by about 2%

compared with using the previously recommend MACSs (KADoNiS-0.3 [44]).

V. SUMMARY

We have measured $^{76}\text{Ge}(n, \gamma)$ cross section over a wide neutron energy range at the neutron time-of-flight facility n_TOF at CERN. Resonance capture kernels of 41 resonances were determined up to 52 keV, 39 of them are listed for the first time. We have determined Maxwellian-averaged cross sections for $k_B T$ values of 5–100 keV, combining our experimental data with theoretical predictions of the cross section at higher energy. The uncertainty of the MACSs from our data is smaller than 5.5% and it is dominated by the systematic uncertainty (of 5.1%). We have also tested the impact of the new MACS on the ^{76}Ge production during s -process nucle-

osynthesis. The results indicate that the ^{76}Ge abundance is underestimated by about 2% in comparison with the previous data.

ACKNOWLEDGMENTS

This work was supported by the Austrian Science Fund FWF (J3503), the Adolf Messer Foundation (Germany), the UK Science and Facilities Council (ST/M006085/1), and the European Research Council ERC-2015-StG No. 677497. We also acknowledge support of Narodowe Centrum Nauki (NCN) under the grant (UMO-2016/22/M/ST2/00183) and University of Lodz under the grant (9/IDUB/MLOD/2021), MEYS of the Czech Republic, the Charles University project UNCE/SCI/013, and the Croatian Science Foundation under the project IP-2018-01-8570.

-
- [1] R. Reifarth, C. Lederer, and F. Käppeler, *J. Phys. G* **41**, 053101 (2014).
- [2] M. Pignatari *et al.*, *Astrophys. J.* **710**, 1557 (2010).
- [3] U. Frischknecht *et al.*, *Mon. Not. R. Astron. Soc.* **456**, 1803 (2016).
- [4] D. Watson *et al.*, *Nature (London)* **574**, 497 (2019).
- [5] K. H. Ackermann *et al.*, *Eur. Phys. J. C* **73**, 2330 (2013).
- [6] N. Abgrall *et al.*, *Adv. High Energy Phys.* **2014**, 365432 (2014).
- [7] N. Abgrall *et al.*, *AIP Conf. Proc.* **1894**, 020027 (2017).
- [8] M. Dolinski *et al.*, *Annu. Rev. Nucl. Part. Sci.* **69**, 219 (2019).
- [9] G. Meierhofer, P. Grabmayr, L. Canella, P. Kudejova, J. Jolie, and N. Warr, *Eur. Phys. J. A* **48**, 20 (2012).
- [10] E. der Mateosian and M. Goldhaber, *Phys. Rev.* **108**, 766 (1957).
- [11] H. Pomerance, *Phys. Rev.* **88**, 412 (1952).
- [12] L. Seren *et al.*, *Phys. Rev.* **72**, 888 (1947).
- [13] K. Maletski *et al.*, *At. Energ. USSR* **24**, 173 (1968).
- [14] D. A. Brown *et al.*, *Nucl. Data Sheets* **148**, 1 (2018).
- [15] A. Plompen, Announcing JEFF-3.3 Release, Technical Report JEFFDoc-1864 (2017).
- [16] J. A. Harvey and M. Hockaday, EXFOR Entry 13770.004, <https://www-nds.iaea.org/exfor/servlet/X4sGetSubent?reqx=11713&subID=13770004&plus=2>
- [17] M. Bhide *et al.*, *Phys. Lett. B* **741**, 150 (2015).
- [18] A. J. Koning *et al.*, *Nucl. Data Sheets* **155**, 1 (2019).
- [19] J. Marganec, I. Dillmann, C. Domingo Pardo, F. Kappeler, R. Reifarth, R. Gallino, M. Pignatari, and P. Grabmayr, *Phys. Rev. C* **79**, 065802 (2009).
- [20] Z. Bao *et al.*, *At. Data Nucl. Data Tables* **76**, 70 (2000).
- [21] R. P. Anand *et al.*, *Nuovo Cimento A* **50**, 247 (1979).
- [22] A. K. Chaubey and M. L. Sehgal, *Nucl. Phys. A* **117**, 545 (1968).
- [23] C. Guerrero *et al.* (n_TOF Collaboration), *Eur. Phys. J. A* **49**, 27 (2013).
- [24] R. Plag, M. Heil, F. Käppeler, P. Pavlopoulos, R. Reifarth, and K. Wisshak, *Nucl. Instrum. Methods Phys. Res. Sect. A* **496**, 425 (2003).
- [25] P. F. Mastinu *et al.*, New C_6D_6 detectors: Reduced neutron sensitivity and improved safety, n_TOF-PUB-2013-002; CERN-n_TOF-PUB-2013-002 (2013).
- [26] P. Zugec *et al.* (n_TOF Collaboration), *Nucl. Instrum. Methods Phys. Res. Sect. A* **812**, 134 (2016).
- [27] R. L. Macklin and R. H. Gibbons, *Phys. Rev.* **159**, 1007 (1967).
- [28] S. Agostinelli *et al.* (Geant4 Collaboration), *Nucl. Instrum. Methods Phys. Res. Sect. A* **506**, 250 (2003).
- [29] F. Bečvář, *Nucl. Instrum. Methods Phys. Res. Sect. A* **417**, 434 (1998).
- [30] U. Abbondanno and the n_TOF Collaboration, *Nucl. Instrum. Methods Phys. Res. Sect. A* **521**, 454 (2004).
- [31] M. Barbagallo and the n_TOF Collaboration, *Eur. Phys. J. A* **49**, 156 (2013).
- [32] R. L. Macklin, J. Halperin, and R. R. Winters, *Nucl. Instrum. Methods* **164**, 213 (1979).
- [33] N. Larson, *Updated Users Guide for SAMMY: Multilevel R-Matrix Fits to Neutron Data Using Bayes Equations*, Technical Report ORNL/TM-9179/R8 (Oak-Ridge National Laboratory, Oak Ridge, TN, 2008).
- [34] A. Gawlik *et al.*, *Phys. Rev. C* **100**, 045804 (2019).
- [35] C. Lederer-Woods *et al.*, *Phys. Lett. B* **790**, 458 (2019).
- [36] M. Dietz *et al.*, *Phys. Rev. C* **103**, 045809 (2021).
- [37] S. F. Mughabghab, *Atlas of Neutron Resonances*, 6th ed. (Elsevier, Amsterdam, 2018).
- [38] Till von Egidy and D. Bucurescu, *Phys. Rev. C* **72**, 044311 (2005).
- [39] R. Capote *et al.*, *Nucl. Data Sheets* **110**, 3107 (2009).
- [40] T. Rauscher and F. K. Thielemann, *At. Data Nucl. Data Tables* **79**, 47 (2001).
- [41] R. Reifarth *et al.*, *Eur. Phys. J. Plus* **133**, 424 (2018).
- [42] C. Lederer *et al.*, *Phys. Rev. C* **83**, 034608 (2011).
- [43] C. Massimi *et al.*, *Eur. Phys. J. A* **50**, 124 (2014).
- [44] I. Dillmann, M. Heil, F. Käppeler, R. Plag, T. Rauscher, and F. K. Thielemann, KADoNiS–The Karlsruhe Astrophysical Database of Nucleosynthesis in Stars, AIP Conf. Proc. 819, p. 123; online at <http://www.kadonis.org>.
- [45] C. Ritter, F. Herwig, R. Hirschi, S. Jones, C. Fryer, and M. Pignatari, *Mon. Not. R. Astron. Soc.* **480**, 538 (2018).
- [46] F. Herwig *et al.*, *PoS (NIC X)* **053**, 023 (2009).